Pramana – J. Phys. (2020) 94:111
https://doi.org/10.1007/s12043-020-01977-y

Numerical analysis of ultrathin Cu(In,Ga)Se_2 solar cells with Zn(O,S) buffer layer

G L MBOPDA TCHEUM[1,3,*], A TEYOU NGOUPO[1], S OUÉDRAOGO[2], N GUIRDJEBAYE[1] and J M B NDJAKA[1]

[1]Faculty of Sciences, Department of Physics, University of Yaounde I, 812 Yaounde, Cameroon
[2]Laboratoire de Matériaux et Environnement (LAME), UFR-SEA, Université Joseph Ki-Zerbo, 03 B.P. 7021 Ouaga 03, Ouagadougou, Burkina Faso
[3]Institut für Festkörperphysik, Friedrich-Schiller-Universität Jena, Max-Wien-Platz 1, 07743 Jena, Germany
*Corresponding author. E-mail: mbopdagabin@gmail.com

MS received 14 October 2019; revised 27 February 2020; accepted 23 April 2020

Abstract. We performed an investigation on the behaviour of the electrical parameters of ultrathin Cu(In,Ga)Se_2 (CIGS) solar cells buffered with Zn(O,S). Using one-dimensional simulations and by defining a new structure, we achieved a significant reduction of the absorber and the buffer layers to evaluate the changes in the cell's performance. The simulation results revealed that a good optimisation of the thickness and sulphur content of the Zn(O,S) buffer layer could be an ingenious way to reduce the thickness of the absorber without compromising the performance of the solar cells. A high efficiency of 16.9% is obtained for 0.5 μm of the absorber layer when the thickness and sulphur content of the Zn(O,S) layer are 10 nm and 0.9 respectively. At this configuration, we introduced p^+-CIGS and SnS layers at the CIGS/Mo interface as back surface field (BSF) to reduce interface recombinations, which are very predominant in ultrathin absorber. An improvement of 2% and 5.96% on the efficiency is obtained with the p^+-CIGS and SnS layers respectively. The shape of the band diagram shows good alignment and low band bending at the CIGS/OVC/Zn(O,S) interfaces and the corresponding conduction band offset is +0.2 eV between the CIGS and the Zn(O,S) layers. Ultrathin CIGS and Zn(O,S) layers can be helpful in improving the stability of the cell with regard to the results obtained from the electrical parameters.

Keywords. Thin films; Zn(O,S); band alignment; back surface field; solar cell capacitance simulator-1-dimension.

PACS No. 68.55.Ln

1. Introduction

Cu(In,Ga)Se_2 absorbers, also known as CIGS, are very important thin film solar cells for converting Sun's energy into electricity; they have reached a record efficiency of over 22.6% [1] typically using cadmium sulphide (CdS) as the buffer layer. The associated technology is a promising option in industrial productivity, due to its lower manufacturing cost and higher efficiency [2]. However, developing cadmium-free (Cd-free) buffer layer for CIGS solar cells is significant in solving environmental issues. Indeed, in September 2013, the European Union registered CdS as a substance of very high concern, due to its carcinogenicity [3]. Therefore, restrictions for its usage are likely to occur in the future despite its broad range of application in CdTe solar cells [4] as in CIGS. The photovoltaic (PV) community has done many studies, to find Cd-free buffer layers and among the alternative buffer layers, zinc oxysulphide (Zn(O,S)) stands as a promising candidate to substitute CdS. It drew the attention of the PV community within the last decade, especially because of its wider band gap [5]. A record efficiency of 20.9% has been achieved using Zn(O,S) buffer layer [6]. However, the main problem related to the usage of Zn(O,S) as the buffer layer in CIGS modules, is the stability of the solar cell. Stability is affected by both the deposition process of the buffer layer, and by the band alignment between CIGS/Zn(O,S)/window layer. According to Naghavi *et al* [7], the nature and the deposition process of the Zn(O,S) buffer layer and the undoped window layer affect the stability and the efficiency of the solar cell. In this work, we present a new solar structure, in which we suggest the reduction of the thicknesses of the

Published online: 24 July 2020

CIGS-absorber and Zn(O,S)-buffer layers as a way of improving their deposition time and then, we address the influence of sulphur content in ultrathin device. We present the influence of such reductions on the electrical properties of the device. Different groups have studied ultrathin CIGS solar cells experimentally in the last decade [8-11], but most of them focussed on reducing only the absorber thickness, without considering the buffer layer. Platzer-Björkman *et al* [12] showed how the variation of Zn(O,S) thickness and oxygen concentration influence the energy band alignment. But they performed their investigations without considering the advantages of reducing the absorber thickness while in this work, we take a look at those considerations. We address the advantages of adding a back surface field (BSF) layer between the ultrathin absorber and the back contact. A few studies pointed out the effect of a BSF layer in ultrathin CIGS solar cell [13–15], but none of them investigate those effects in ultrathin CIGS solar cells with Zn(O,S) buffer layer.

2. Device model and simulation details

The investigated cell structure is a stack of several layers with various thicknesses, built as presented in figure 1. The layer between the absorber and the buffer layers is the ordered vacancy compound (OVC) layer. Its growth on the surface of CIGS films is beneficial to the performance of the cells because, at the buffer/absorber interface, it moves the electrical junction away from high recombination [16]. MgF_2 acts as an antireflection layer, thus increases photons absorption. Discussion about the other layers included in our cell are available in [13,17].

We simulated the cell structure of figure 1b using the one-dimensional simulation program solar cell capacitance simulator version 3.3.00 (SCAPS-1D) [18]. SCAPS-1D program calculates the internal electrical parameters of CIGS solar cells by solving the Poisson's equation, as well as electrons and holes continuity equations. Recombination currents are calculated using the Shockley–Read–Hall (SRH) model for bulk defects and an extension of the SRH model for interface defects. Simulations can investigate the effects of doping concentration, free carrier mobility, band gap, structural properties and layer thicknesses on device performance. The material parameters used as initial input for simulations are given in table 1. However, the properties of the absorber layer have been taken from [19]. The default illumination spectrum is set to the global AM1.5 standard and the influence of the series resistance is not considered. The temperature and the incident light power (P_s) have been set equal to 300 K and 1000 W/m^2 respectively. In the first part of our simulations, we do not consider the BSF layers.

3. Results and discussion

3.1 *Comparison with experimental results*

Figure 2 shows the J–V characteristics of our solar cell of figure 1b using the data of table 1 and the J–V characteristics obtained using experimental data. We defined the thickness of the absorber layer to be 2.5 μm as in the experiment and doping concentration to be 2×10^{16} cm^{-3}. In our previous paper, we calibrated the program to reproduce exactly the experimental result with the CdS layer. We used this previous model by replacing the CdS layer by the Zn(O,S) layer [19]. The discrepancy observed in the parameters of the J–V characteristic when the CdS layer is replaced by the Zn(O,S) layer, mainly the higher short-circuit current density, is due to the wide band gap of the Zn(O,S) buffer layer compared to the CdS layer, contributing to the limitation of the losses caused by high-energy photon absorption in CdS. Moreover, this discrepancy can also originate from the cells area, which is set to 1 cm^2 in our simulation package and half for the experimental samples. In table 2, we present and compare the obtained results with those obtained experimentally by Jackson *et al* [1] for the standard CdS. The fill factor (FF) is close to the one obtained experimentally. However, the difference noticed in open circuit voltage (V_{oc}) is obviously due to the recombination of charge carriers, which occur in the bulk of the absorber, at the buffer/absorber interface and at the back contact. Thus, the J–V characteristics of the experimental data and our simulation have the same trend, and the obtained results validate our set of data as baseline for simulation and confirm Zn(O,S) as an alternative to CdS.

3.2 *Influence of the thickness of the absorber on electrical parameters*

In this section, we discuss the influence of the thickness of the absorber and doping, on the electrical parameters of the cell; beforehand, we set the buffer layer thickness at 50 nm as it is commonly set in experiments. We can see in figure 3a that V_{oc} is dependent more on the variation of the doping concentration and less on the absorber thickness. It can even reach very important values which are greater than 0.85 V. This enhancement may be attributed to dopants which increase the acceptor and free carrier concentration by passivating defects and reducing interdiffusion of elements in the absorber. Tokio Nakada [20] reported, for the case of Na elements

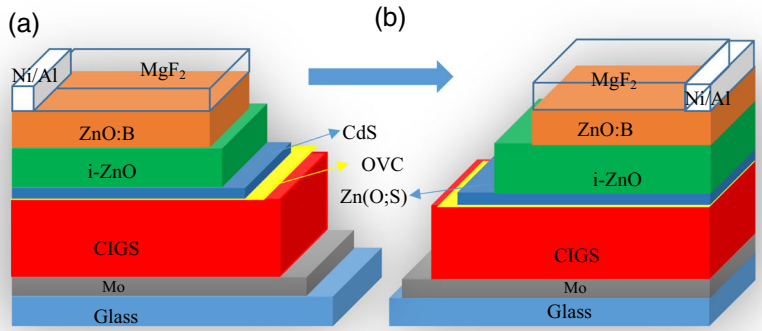

Figure 1. Structures of CIGS-based solar cell used in the simulation: the CdS layer is replaced by a Cd-free layer.

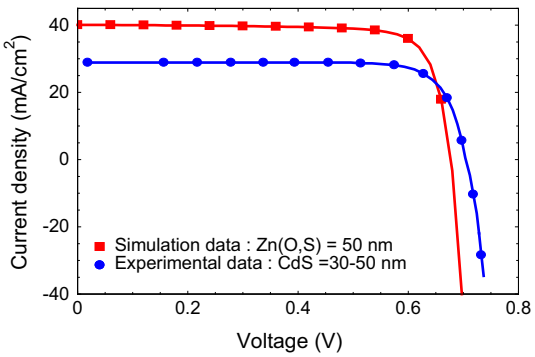

Figure 2. Comparison of current–voltage simulation curve with experimental data of ref. [1].

for instance, their effects on CIGS structure as a reason of V_{oc} enhancement. Additionally, according to Anderson's model used in SCAPS-1D for the calculation of conduction (ΔE_C) and valence (ΔE_V) band offset [21], $\Delta E_V \geq 0.15$ eV at the CIGS/OVC interface, leads to the highest V_{oc} by suppressing the interface recombination. This result is in good agreement with the work of Nishimura *et al* [22]. For doping concentrations of 10^{17} cm^{-3} and 10^{18} cm^{-3}, V_{oc} coincide. At these doping levels, the supplementary carriers are no longer collected and are recombined as soon as generated because of the suboptimal band alignment at the absorber–buffer interface. However, we surprisingly observe a large increase of V_{oc} for doping concentrations higher than 10^{18} cm^{-3}. We are tempted to believe, from our simulations that, the doping concentration can enhance band alignment at the CIGS/Zn(O,S) interface, as the generally low value of V_{oc} in CIGS solar cells buffered with Zn(O,S) layers is due to the suboptimal band alignment at the buffer/absorber interface [23].

On the other hand, the trend of FF depends on whether the doping concentration is less or greater than 10^{15} cm^{-3} (figure 3b). In fact, FF sharply decreases with the thickness of the absorber layer when the doping concentration is below 10^{15} cm^{-3} and it remains almost constant for a doping concentration greater than this. To analyse FF losses, we have used empirical expression that relates FF to V_{oc} and the quality factor A (eq. (1)) [24].

$$\mathrm{FF} = \frac{v_{oc} - \ln(v_{oc} + 0,72)}{v_{oc} + 1} \tag{1}$$

where $v_{oc} = qV_{oc}/AkT$.

According to this equation, the losses of FF are related to those of V_{oc}; they are mainly due to bulk recombination and granular structure which impede, at low doping concentration, the collection of charge carriers. Increasing the absorber thickness with such doping level would bring more defects and not enough dopants, leading to transient effects on the cell's performance. This could explain the drop of J_{sc} with the increasing thickness observed under 10^{15} cm^{-3} in figure 3c.

The short-circuit current (J_{sc}) shows the same trend as V_{oc} for low doping concentrations (see figure 3c). However, a high doping level of the absorber layer leads to an increase in J_{sc} with thickness. The loss of J_{sc}, in the doping concentration range of 10^{16}–10^{20} cm^{-3} is due to the amount of charge carriers brought in the bulk of the absorber by doping. Moreover, the reduction of the space charge region due to the high doping level could be one reason for this loss [25]. Indeed, in ultrathin layers, a high doping level increases the concentration of carriers and then the probability of carrier collision. Therefore, the mobility of charge carriers decreases by increasing consequently the recombination, and hence the low values of J_{sc}. However, in thicker absorber layers, the collision phenomenon diminishes leading to the increase of J_{sc}. When the doping concentration is 10^{15} cm^{-3}, J_{sc} shows no dependency on the thickness and its value is about 35 mA/cm^2. This result is 5 mA/cm^2

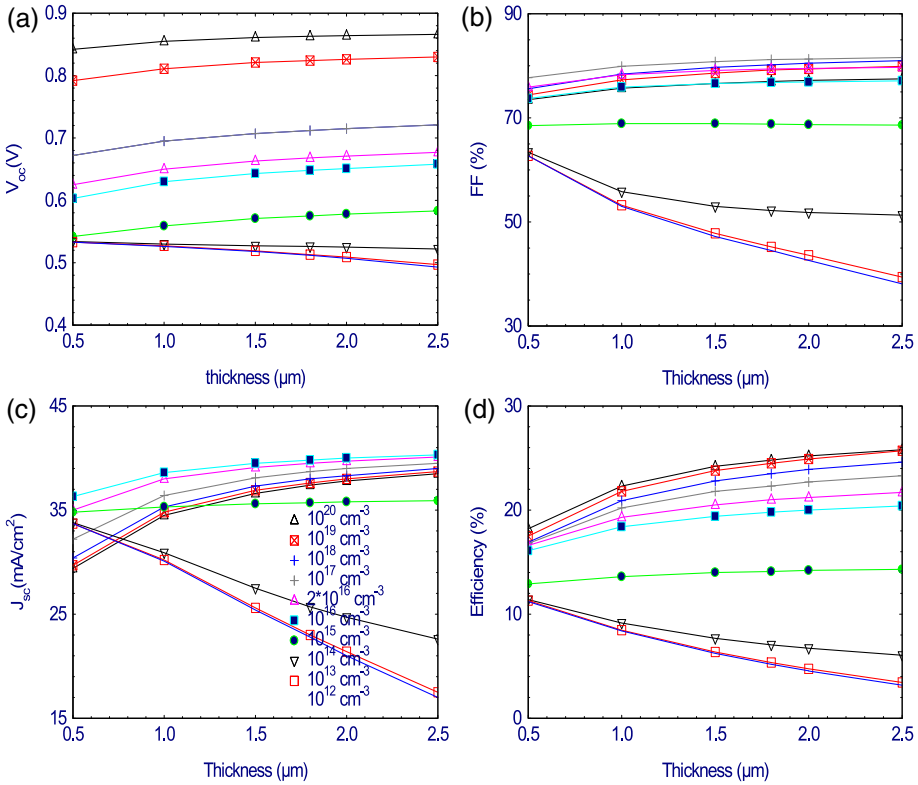

Figure 3. Variation of the electrical parameters with respect to the thickness according to the doping concentration.

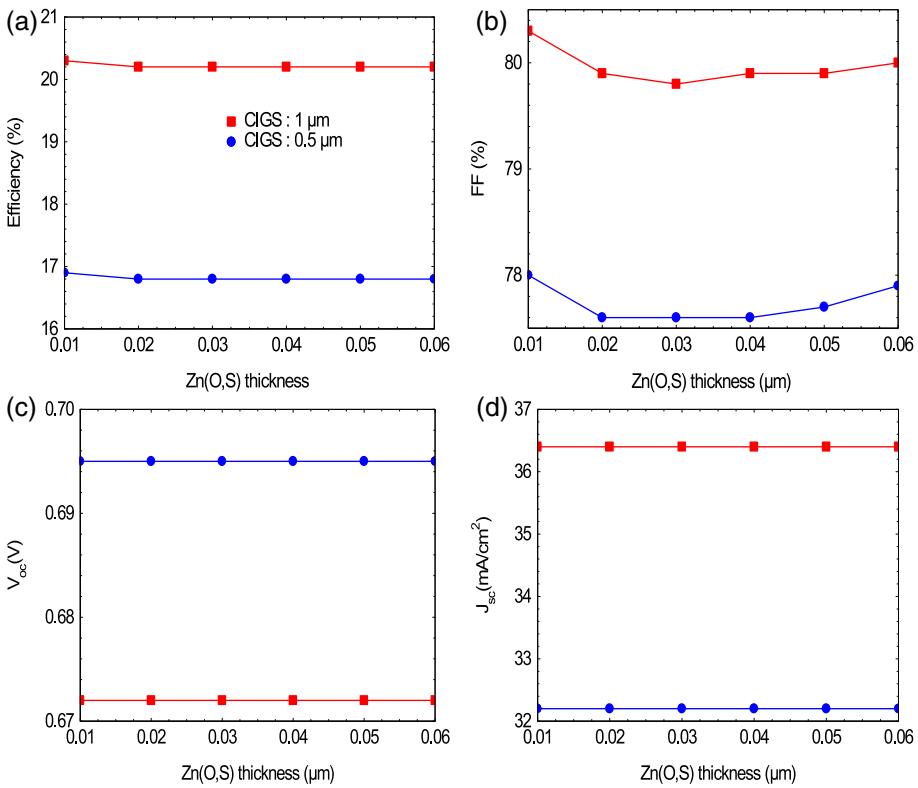

Figure 4. Influence of Zn(O,S) thickness on the electrical parameters according to the CIGS thickness.

Table 1. Parameters used for the simulation of different configurations.

			Layers			
Layers properties	SnSe/P^+-CIGS (BSF)	CIGS [19]	OVC [13]	Zn(O,S)	i-ZnO [13]	ZnO:B [13]
Layer thickness: w (nm)	10	Variable	30	Variable	200	400
Layer band gap: E_g (eV)	1.25/1.1	1.15	1.3	Graded	3.3	3.3
Electron affinity: χ (eV)	4.2/4.5	4.5	4.5	4.3	4.55	4.55
Dielectric relative permittivity: $\varepsilon/\varepsilon_1$	12.5/13.6	13.6	13.6	10	9	9
Conduction band effective density of states: N_c (cm^{-3})	$1\times10^{19}/2\times10^{18}$	2.2×10^{18}	2.2×10^{18}	2.2×10^{18}	3.1×10^{18}	3×10^{18}
Valence band effective density of state: N_v (cm^{-3})	$4.13\times10^{19}/1.8\times10^{18}$	1.5×10^{19}	1.5×10^{18}	1.8×10^{19}	1.8×10^{19}	1.8×10^{19}
Electron thermal velocity: v_e (cm/s)	10^7	3.9×10^7	3.9×10^7	3.1×10^7	2.4×10^7	2.4×10^7
Hole thermal velocity: v_h (cm/s)	10^7	1.4×10^7	1.4×10^7	1.6×10^7	1.3×10^7	1.3×10^7
Electron mobility: μ_e (cm^2/Vs)	25/100	100	10	100	100	100
Hole mobility: μ_h (cm^2/Vs)	100/25	12.5	1.25	25	31	31
Doping concentration (cm^{-3})	$6x10^{18}/10^{18}$ (a)	Variable (a)	10^{13} (a)	10^{17} (d)	10^{17} (d)	10^{20} (d)
			Bulk defects properties			
Defect density and type: N (cm^{-3})		10^{14}(D)	10^{14}(D)	5×10^{16}(A)	10^{16}(A)	10^{16}(A)
Capture cross-section electrons: σ_e (cm^2)		10^{-15}	10^{-15}	10^{-15}	10^{-15}	10^{-15}
Capture cross-section holes: σ_h (cm^2)		10^{-11}	10^{-11}	5×10^{-13}	5×10^{-13}	5×10^{-13}
			Interfaces properties			
Interface state		CIGS/OVC			OVC/Zn(O,S)	
Interface conduction band offset: ΔE_c (eV)		0.0			0.2	
Defect density and type: N (cm^2)		10^{11}(N)			3×10^{13}(N)	
Capture cross-section electrons: σ_e (cm^2)		10^{-15}			10^{-15}	
Capture cross-section holes: σ_h (cm^2)		10^{-15}			10^{-15}	

(a) and (d) stand for shallow acceptor and donor defects respectively, while (A), (D) and (N) are deep acceptor, donor and neutral defects respectively.

Table 2. Comparison between simulation and experimental data of ref. [1].

	Thickness (nm)	V_{oc} (V)	J_{sc} (mA/cm^2)	FF (%)	Efficiency (%)
Simulation data with Zn(O,S)	50	0.677	40.13	79.73	21.68
Experimental data with CdS	30–50	0.741	37.8	80.6	22.6

greater than that of the standard CdS reported in [26]. All the other electrical parameters are almost constant at 10^{15} cm^{-3} doping concentration.

Furthermore, the doping concentration enhances the efficiency as one can see in figure 3d. But it drops significantly for doping concentration below 10^{15} cm^{-3}. This is a consequence of the variation of FF, V_{oc} and J_{sc} as shown in eq. (2). Between 0.5 μm and 1.5 μm, efficiencies up to 21.5% can be achieved with a doping concentration of 10^{17} cm^{-3}. This result on the efficiency would be even greater if the band alignment at the buffer/absorber interface is optimised. Although we obtain a better result of the efficiency with doping concentration greater than 10^{17} cm^{-3}, their effects on the other electrical parameters (FF and J_{sc}) are detrimental for the cell at ultrathin layers.

$$\eta = \frac{\mathrm{FF} * V_{oc} * J_{sc}}{P_s}. \quad (2)$$

With regard to the previous results, V_{oc} and FF are more dependent on the doping concentration, while J_{sc} depends much more on the absorber thickness. But high values of those electrical parameters can be obtained using ultrathin absorber.

3.3 *Buffer properties*

The results obtained above show that, using 1 μm of the absorber and an average doping concentration of 10^{17} cm^{-3}, an efficiency of 20.2% can be achieved. Thus, the thickness ranging from 0.5 to 1 μm looks optimal for reaching high efficiencies with ultrathin absorber. In this section and for 0.5–1 μm thickness range, we investigated the changes in electrical parameters when the buffer thickness is also reduced and we showed the influence of sulphur content in ultrathin device.

3.3.1 *Influence of buffer thickness on the electrical parameters.* There is a slight increase in FF and efficiency when the thickness of the buffer layer decreases (η=20.3% when the thickness of Zn(O,S) layer = 10 nm), while V_{oc} and J_{sc} remain constant as shown in figure 4. This may be due to the fact that, the reduction of the buffer layer does not affect the width of the space charge region in the CIGS layer. Then, there is no loss of free charge careers and their collection is slightly improved. The thickness of the Zn(O,S) layer can also be decreased from 50 nm to 10 nm without losses in the cell's performance, if the CIGS absorber is only

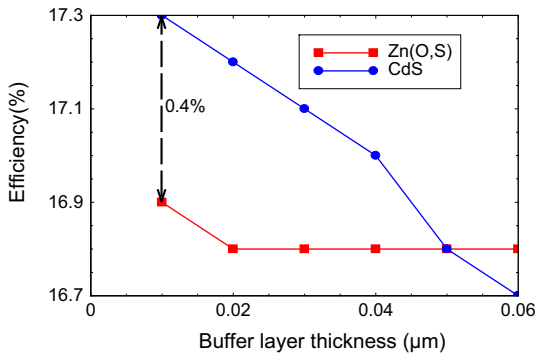

Figure 5. Comparison of efficiencies of CIGS cells buffered Zn(O,S) and CdS at 0.5 μm absorber thickness.

0.5 μm thick. The corresponding efficiency of 16.9% is close to the one obtained with a same thickness of the standard CdS (figure 5). Indeed the reduction of the CdS layer to 10 nm, as is the case with Zn(O,S), leads to an efficiency of 17.3% which is only 0.4% higher than the efficiency of the cell with Zn(O,S). However, the doping profile shows a high density of charges in the depletion region (figure 6), which may originate from the presence of defects in the absorber layer. These defects increase the band bending at the absorber–buffer interface and increase recombination, hence the drop of charge carriers. Indeed, photogenerated charges are strongly recombined close to the p-area of the depletion region and are probably tunnelling assisted. But, close to the interface, we notice a uniform distribution of charges although they decrease in density. This homogenisation of charges toward the interface is the proof of a relatively good band alignment in spite of the bending effect induced by the defects in the p-area of the depletion region. It also explains the constancy of J_{sc} and V_{oc} obtained with the decrease of the buffer layer.

3.3.2 *Influence of the band-gap energy on the electrical parameters.* The sulphur content in the buffer layer can affect its band-gap energy, as shown in eq. (3) [27], in which we assumed that the contribution of hydroxides is negligible. E_{ZnS} = 3.6 eV and E_{ZnO} = 3.2 eV are the energy band gaps of the binary compounds, b ~3.1 eV [5] is the optical bowing parameter and x is the sulphur content. The bowing effect results in different behaviours of the valence band maximum and the conduction band minimum relative to x [28]. For ultrathin Zn(O,S) layers, the sulphur content in the buffer layer

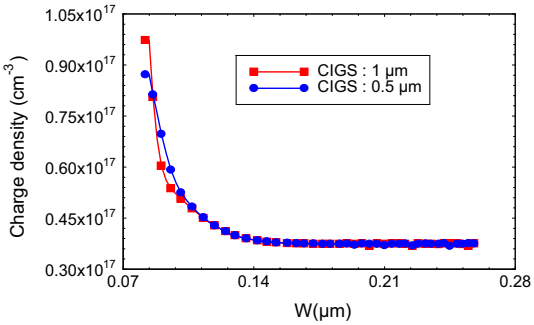

Figure 6. Doping profile of the cell.

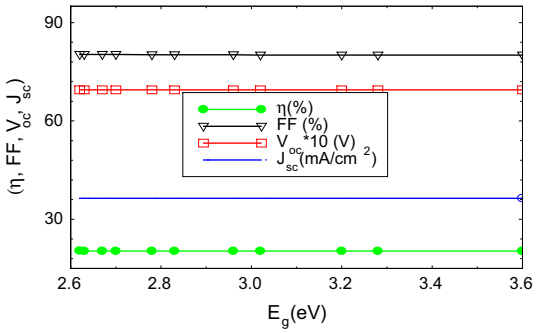

Figure 7. Variation of electrical parameters with the band–gap energy.

has no significant effect on the electrical parameters (figure 7), and the modifications it implies on the optical properties, through the band-gap variation, seem to have no beneficial or detrimental effect on the cell's properties as they remain constant when the sulphur content varies. Indeed, at this thickness range, the Zn(O,S) buffer layer is not thick enough to have an effective control of the conduction band offset (CBO) at CIGS/Zn(O,S) interface. Therefore, the change of band-gap energy would not lead to significant change in conduction band and therefore in the solar properties. Nevertheless, when x is set between 0.6 and 0.9 (figure 8) recombination currents diminish leading to an increase in the direct current of the junction. Indeed, recombination currents cause the variation of hole and electron currents while crossing the depletion region. This variation, which is due to the generation and recombination occurring in the depletion region, cuts down or increases the direct current at the junction. In the latter range of x, the sulphur content improves the generation phenomena of free carriers in the depletion region and hence decreasing the recombination current in that range. This explains the slight increase of η and FF in figures 4a and 4b. The constancy of the electrical parameters of ultrathin devices can be helpful for improving the deposition time of the Zn(O,S) buffer layer on CIGS samples and the results obtained are encouraging in replacing the standard CdS by Zn(O,S).

$$E_{\mathrm{Zn(O,S)}} = x E_{\mathrm{ZnS}} + (1-x) E_{\mathrm{ZnO}} - b(1-x)x. \quad (3)$$

3.4 *Effects of back surface field (BSF)*

In this section, we focussed on the ultrathin absorber of 0.5 μm and we performed numerical analysis of the effects on the cell's performances of two different back surface field (BSF) materials already reported in literature [14,15]: tin selenide (SnSe) and a highly doped CIGS layer (known as p^+-CIGS layer). Indeed, the ultrathin state of the absorber layer increases recombination of minority carriers at the back contact, then it is always of great importance to use a BSF layer to cut down those recombination effects and use an ultrathin absorber. The structure of our solar cell is defined as follows: ZnO:B/i-ZnO/Zn(O,S)/OVC/CIGS/BSF/Mo/substrate (figure 9).

The thickness and the band gap of the buffer layer have been set to 10 nm and 3.2 eV, respectively. We assumed flat band conditions between the BSF and the back contact. Figure 10 presents the current–voltage characteristics of the structures without and with the BSF. Table 3 presents the resulting performances.

The results obviously show that, the BSF has beneficial effects on the cell's performance, but each of them does not have the same effect on the cell. The addition of a BSF layer cuts down the recombination and increases charge collection, hence the increase of V_{oc} (table 3). SnSe seems more beneficial to the cell than the p^+-CIGS layer as it leads to the highest electrical parameters. Moreover, its cell's efficiency is less adjustable by doping than the one with p^+-CIGS layer (figure 11). The efficiency obtained is comparable to the one obtained by Jackson *et al* [1]. More interestingly, we obtained this efficiency of 22.86% with an ultrathin CIGS layer of 0.5 μm and a buffer layer of 10 nm only, while the results obtained experimentally needed an absorber thickness of 2.5–3 μm and a buffer thickness of 30–50 nm, thanks to the BSF, which repels the charge carriers from recombination at the back contact by modifying the states' interfaces between the absorber and the back contact. However, the cell structure with SnSe is less stable than the one with p^+-CIGS layer. Indeed, the efficiency drops for both structures (figure 11) as the temperature varies and the average decreasing rate is 2.78% and 1.36% in the cell structure with SnSe and p^+-CIGS layers respectively. The low stability of the cell with SnSe is due to the atomic diffusion and mainly to the strong band bending at the SnSe/absorber interface (figure 12a). Indeed, an electron barrier is formed near the SnSe/absorber interface due to the shift of the

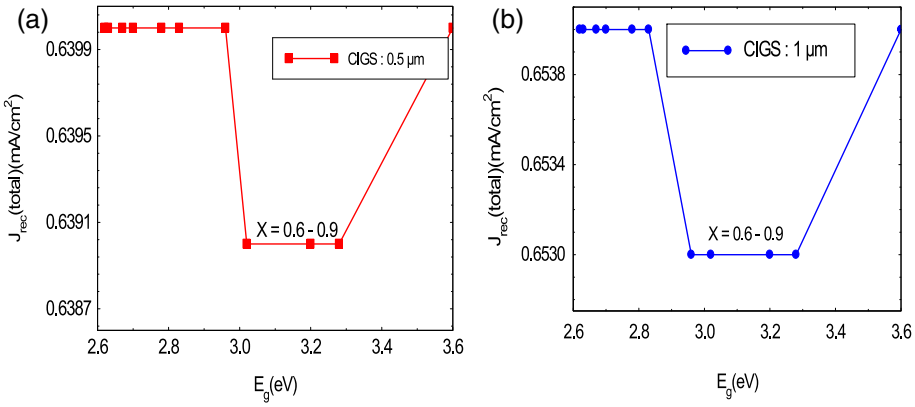

Figure 8. Variation of the total recombination current with the band-gap energy.

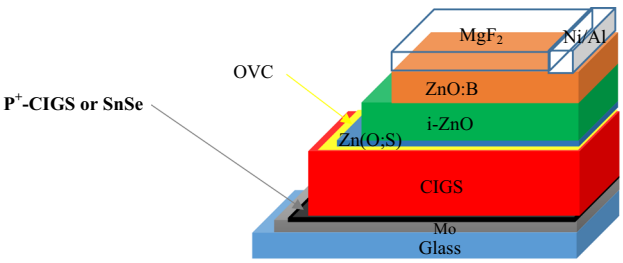

Figure 9. Structure of the CIGS-based solar cell with BSF.

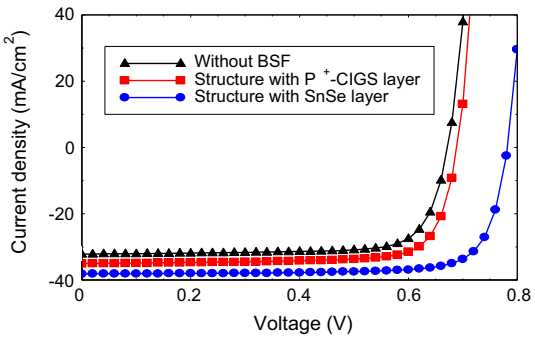

Figure 10. Current–voltage characteristics of the structures without and with different BSF layers.

Fermi level towards the valence band maximum. Hence, a strong bending is observed in figure 11a. Actually, the p^+-CIGS/absorber interface does not lead to such a strong band bending because both layers are made of the same material. Therefore, defect states are less at that interface (figure 12b).

In both structures, CBO at the CIGS/Zn(O,S) interface is +0.2 eV. There is a low band bending between the buffer, the OVC and the absorber's conduction band, because of the uniform distribution of charge carriers observed in figure 6 leading then, to a good transfer and collection of charge carriers. However, the spike at the buffer's conduction band (figures 12a and 12b) can act as carrier traps and as high recombination area; but regarding the band alignment at Zn(O,S)/OVC interface, charge carriers would unlikely be trapped at that interface. The good band alignment observed can also explain why there is no variation of V_{oc} and J_{sc} in ultrathin absorber and buffer layers (figures 4c and 4d). The range of optimal CBO at room temperature is approximately 0.1–0.4 eV [29,30], and our result is then in good agreement with the last result. Moreover, the obtained result is not far from the one ((0.09 ± 0.02) eV) obtained by Mezher *et al* [31]. On the other hand, the abrupt valence band offset (VBO) at the OVC/buffer interface is due to the wide band gap of the buffer and window layers with respect to those of the absorber; but this high VBO has no influence on carrier collection.

4. Conclusion

We performed an investigation on the electrical properties of CIGS solar cells with Zn(O,S) buffer layer using SCAPS-1D. We showed that, ultrathin absorber in the range of 1–0.5 μm can exhibit high efficiencies up to 20.2% when the buffer layer is 50 nm. Some of the electrical parameters of the cell remain constant when the sulphur content varies and when the Zn(O,S) layer is reduced from 50 nm to 10 nm, while some of them increase slightly. Indeed, with only 10 nm thick Zn(O,S) layer, we obtained efficiencies of 20.3% and 16.9% using CIGS absorber thicknesses of 1 μm and 0.5 μm, respectively. However, the efficiency dramatically increases to 18.91% and 22.86% by introducing a p^+-CIGS layer and a SnSe layer as BSF respectively, but the cell with the SnSe is less stable than the one with the p^+-CIGS layer. The total recombination current drops when the sulphur content is set between 0.7 and 0.9 and the band diagram of our numerical sample has a

Table 3. Electrical parameters of the cell's structures with and without BSF.

	V_{oc} (V)	J_{sc} (mA/cm^2)	FF (%)	Efficiency (%)
Without BSF	0.672	32.2	77.74	16.83
With p$^+$-CIGS layer	.689	35.05	78.25	18.91
With SnSe layer	.761	37.75	79.46	22.86

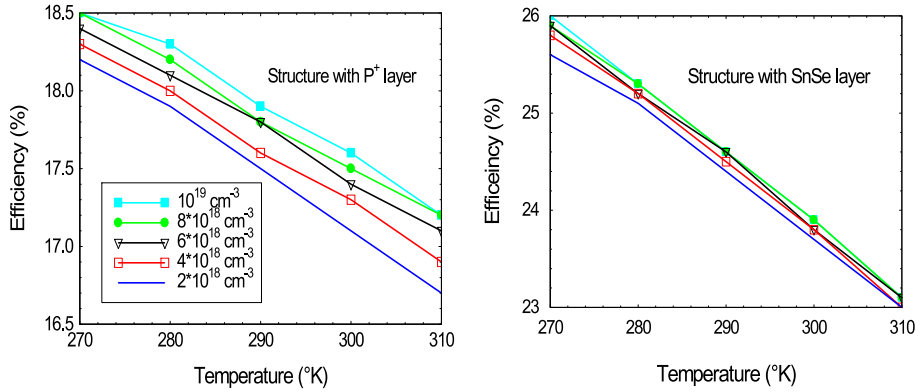

Figure 11. Variation of efficiency with temperature and doping concentration of the BSF.

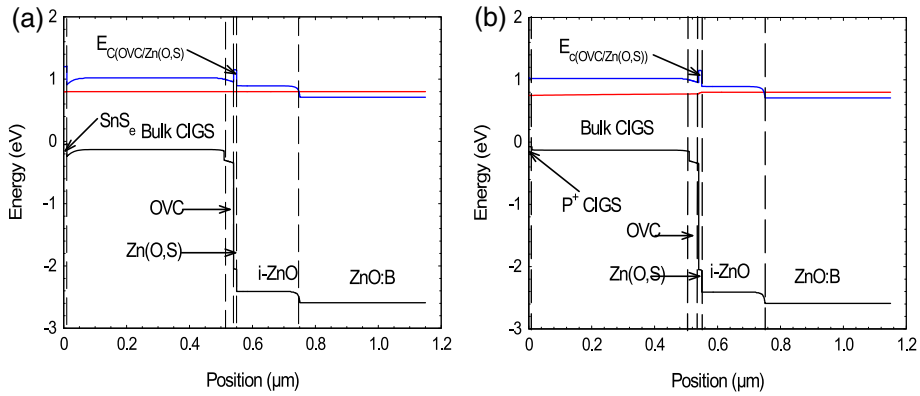

Figure 12. Band energy diagram of the structure with **(a)** SnSe and **(b)** p$^+$-CIGS as BSF.

CBO of +0.2 eV at the CIGS/Zn(O,S) interface. These results on the thickness are relevant as they can lead to the improvement of the deposition time of the Zn(O,S) buffer layer and therefore, improve the efficiency of the cell.

Acknowledgements

The authors acknowledge the German Academic Exchange Service (DAAD) for the funding of the ongoing project. The authors acknowledge Marc Burgelman and colleagues at the University of Gen for making available the simulation program SCAPS-1D. The authors also acknowledge Ms. Laurel Mimboe, for helping them in language correction and writing style.

References

[1] P Jackson, R Wuerz, D Hariskos, E Lotter, W Witte and M Powalla, *Phys. Status Solidi* **10**, 583 (2016)
[2] Md Asaduzzaman, M Hasan and A Newaz Bahar, *SpringerPlus* **5**, 578 (2016)
[3] European Chemicals Agency (ECHA), *Support document for identification of CdS as a substance of very high concern*, https://echa.europa.eu/documents/10162/2aceee75-6b50-416c-aa30-d3131c5eeee3 (2013)
[4] M S Ilango and S K Ramasesha, *Pramana – J. Phys.* **90**: 1 (2018)
[5] M Buffière, S Harel, C Guillot-Deudon, L Arzel, N Barreau and J Kessler, *Phys. Status Solidi A* **212**, 282 (2015)
[6] C Bugot, N Schneider, M Jubault, D Lincot and F Donsanti, *J. Vac. Sci. Technol. A* **33**, 1 (2015)

[7] N Naghavi, T Hildebrandt, M Bouttemy, A Etcheberry and D Lincot, *SPIE: Ox-based Mat. and Dev. VII* **9749**, 97491I (2016)
[8] G Yin, V Brackmann, V Hoffmann and M Schmid, *Sol. Energ. Mat. Sol. C* **132**, 142 (2015)
[9] B Vermang, J T Wätjen, V Fjällström, F Rostvall1, M Edoff, R Kotipalli, F Henry and D Flandre, *Prog. Photovolt*. **22**, 1023 (2014)
[10] K Kim, H Park, W K Kim, G M Hanket and W N Shafarman, *IEEE J. Photovolt.* **3**, 446 (2012)
[11] J Pettersson, T Törndahl, C Platzer-Björkman, A Hultqvist and M Edoff, *J. Photovolt. IEEE* **3**, 1376 (2013)
[12] C Platzer-Björkman, T Törndahl, D Abou-Ras, J Malmström, J Kessler and L Stolt, J. Appl. Phys. **100**, 2 (2006)
[13] S Ouédraogo, F Zougmoré and J M Ndjaka, *Int. J. Photoenergy* **2013**, 1 (2013)
[14] A K Ehemba, M M Socé, J J Domingo, S Cisse and M Dieng, *Am. J. Energy Res*. **5**, 57 (2017)
[15] E I Ahamed, S Bhowmik, M A Matin and N Amin, *Int. Conf. ECCE* (2017) pp. 428–432, https://doi.org/10.1109/ECACE.2017.7912942
[16] A Bouloufa, K Djessas and A Zegadi, *Thin Solid Films* **515**, 6285 (2007)
[17] M D Wanda, S Ouédraogo, F Tchoffo, F Zougmoré and J M B Ndjaka, *Int. J. Photoenergy* **2016**, 1 (2016)
[18] M Burgelman, P Nollet and S Degrave, *Thin Solid Films* **361**, 527 (2000)
[19] S Ouédraogo, F Zougmoré and J M Ndjaka, *J. Phys. Chem. Solids* **75**, 688 (2014)
[20] T Nakada, *Electron. Mater. Lett*. **8**, 179 (2012)
[21] A T Ngoupo, S Ouédraogo and J M Ndjaka, *Indian J. Phys.* **93**, 869 (2019)
[22] T Nishimura, S Toki, H Sugiura, K Nakada and A Yamada, *Prog. Photovolt.* **26**, 291 (2018)
[23] T M Friedlmeier, P Jackson, A Bauer, D Hariskos, O Kiowski, R Wuerz and M Powalla, *IEEE J. Photovolt.* **5**, 1487 (2015)
[24] S H Demtsu and J R Sites, *Conference Record of the Thirty-first IEEE Photovoltaic Specialists Conference* (Lake Buena Vista, FL, USA, USA, 2005)
[25] P Schöppe, S Schönherr, R Würz, W Wisniewski, G M-Criado, M Ritzer, K Ritter, C Ronning and C S Schnohr, *Nano Energy* **42**, 307 (2017)
[26] A Duchatelet, E Letty, S Jaime-Ferrer, P P Grand, F Mollica and N Naghavi, *Sol. Energ. Mat. Sol. C* **162**, 114 (2017)
[27] R Hill, *J. Phys. C* **7**, 521 (1974)
[28] C Persson, C Platzer-Björkman, J Malmström, T Törndahl and M Edoff, *Phys. Rev. Lett.* **97**, 1 (2006)
[29] M Gloeckler, *Device physics of Cu(In,Ga)Se_2 thin-film solar cells*, Ph.D. dissertation (Colorado State University, Fort Collins, CO, USA, 2005)
[30] S Sharbati and J R Sites, *IEEE J. Photovolt.* **4**, 697 (2014)
[31] M Mezher, R Garris, L M Mansfield, K Horsley, L Weinhardt, D A Duncan, M Blum, S G Rosenberg, M Bär, K Ramanathan and C Heske, *Prog. Photovolt.* **24**, 1142 (2016)